The Journal of Chemical Physics

RESEARCH ARTICLE | MAY 09 2024

Flash melting amorphous ice

Special Collection: Water: Molecular Origins of its Anomalies

Nathan J. Mowry ; Constantin R. Krüger ; Gabriele Bongiovanni ; Marcel Drabbels ; Ulrich J. Lorenz

Check for updates

J. Chem. Phys. 160, 184502 (2024)
https://doi.org/10.1063/5.0202948

View Online
Export Citation

14 May 2024 05:17:49

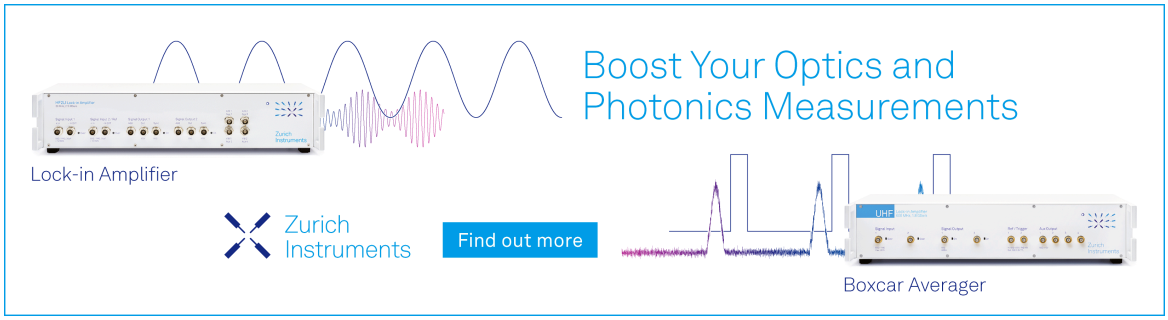

AIP Publishing

The Journal of Chemical Physics ARTICLE pubs.aip.org/aip/jcp

Flash melting amorphous ice

Cite as: J. Chem. Phys. 160, 184502 (2024); doi: 10.1063/5.0202948
Submitted: 8 February 2024 • Accepted: 23 April 2024 •
Published Online: 9 May 2024

View Online Export Citation CrossMark

Nathan J. Mowry, Constantin R. Krüger, Gabriele Bongiovanni, Marcel Drabbels, and Ulrich J. Lorenz[a)]

AFFILIATIONS

Ecole Polytechnique Fédérale de Lausanne (EPFL), Laboratory of Molecular Nanodynamics, CH-1015 Lausanne, Switzerland

Note: This paper is part of the JCP Special Topic on Water: Molecular Origins of its Anomalies.
[a)]**Author to whom correspondence should be addressed:** ulrich.lorenz@epfl.ch

ABSTRACT

Water can be vitrified if it is cooled at high rates, which makes it possible to outrun crystallization in so-called no man's land, a range of deeply supercooled temperatures where water crystallizes rapidly. Here, we study the reverse process in pure water samples by flash melting amorphous ice with microsecond laser pulses. Time-resolved electron diffraction reveals that the sample transiently crystallizes despite a heating rate of more than 5×10^6 K/s, even though under the same conditions, vitrification can be achieved with a similar cooling rate of 10^7 K/s. Moreover, we observe different crystallization kinetics for amorphous solid water and hyperquenched glassy water. These experiments open up new avenues for elucidating the crystallization mechanism of water and studying its dynamics in no man's land. They also add important insights into the laser melting and revitrification processes that are integral to the emerging field of microsecond time-resolved cryo-electron microscopy.

© 2024 Author(s). All article content, except where otherwise noted, is licensed under a Creative Commons Attribution (CC BY) license (https://creativecommons.org/licenses/by/4.0/). https://doi.org/10.1063/5.0202948

14 May 2024 05:17:49

Water is a poor glass former.[1,2] In order to achieve vitrification, it has to be cooled so rapidly that crystallization in so-called no man's land[1] can be outrun, a range of deeply supercooled temperatures between 160 and 232 K, where water crystallizes within tens of microseconds.[3] Critical cooling rates of 3×10^5 K/s (Ref. 4) and 10^6–10^7 K/s have been determined with different methods.[5] In fact, it had long been thought impossible that aqueous solutions could be vitrified,[6] making the demonstration of successful vitrification a stunning achievement.[7,8] Arguably, one of the most important applications of this process is the preparation of samples for cryo-electron microscopy (cryo-EM),[9] which is now set to become the preferred method in structural biology.[10] Vitrification allows biological specimens to be preserved in a frozen-hydrated state, in which they can be imaged in the vacuum of an electron microscope while the damage inflicted by the electron beam is mitigated.[11–13]

Fast crystallization in no man's land had long made it impossible to map out the structural evolution of water during the vitrification process.[3,14–18] Recently, we have used time-resolved electron diffraction to show that water evolves smoothly from a high- to a low-temperature structure between 260 and 220 K.[3] Below 200 K, its diffraction pattern converges to that of hyperquenched glassy water (HGW), a glassy form of water with a glass transition temperature of 136 K.[4] Such smooth evolution had previously also been inferred from the infrared spectra of transiently heated amorphous ices.[19] Here, we study the reverse of the vitrification process by characterizing the structural evolution of different amorphous ices during impulsive laser melting. Laser heating of amorphous ice has frequently been used to prepare deeply supercooled water.[16,19–23] For example, such experiments have provided evidence of a liquid–liquid phase separation in no man's land that can be observed after laser heating of high and low density amorphous ice.[22,23] Recently, we have also introduced a microsecond time-resolved approach to cryo-EM that involves rapidly melting a cryo sample with a microsecond laser pulse.[11,12,24] Once the sample is liquid, a suitable stimulus is used to initiate the dynamics of the embedded proteins. As they unfold, the heating laser is switched off, and the sample revitrifies within microseconds, trapping the proteins in their transient configurations, in which they are subsequently imaged. For example, we have used this approach to image the microsecond motions that the capsid of the cowpea chlorotic mottle virus (CCMV) virus undergoes as part of its infection mechanism.[24] Previous experiments have raised the question of whether cryo samples may partially crystallize during laser melting despite heating rates of about 10^7 K/s.[12,25] This is consistent with previous

© Author(s) 2024

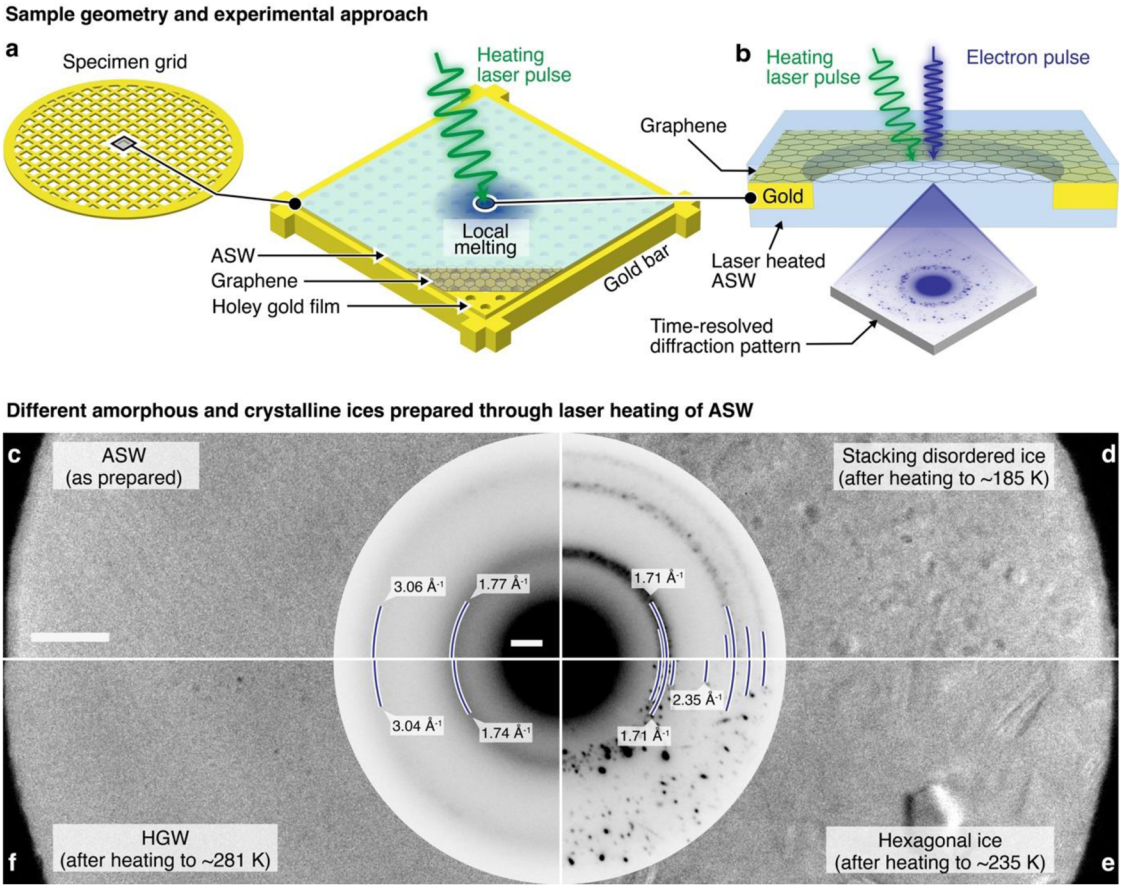

FIG. 1. Illustration of the experimental approach as well as micrographs and diffraction patterns of different amorphous and crystalline ices created in our experiment. (a) Illustration of the sample geometry. A gold mesh supports a holey gold film covered with multilayer graphene. A 263 nm thick layer of ASW is deposited (101 K sample temperature) and locally melted with a 30 μs laser pulse. (b) Diffraction patterns of the structural evolution of the ASW sample during the melting process are captured with intense, 2 μs electron pulses (200 kV accelerating voltage). (c)–(f) Micrographs and diffraction patterns of different amorphous and crystalline ices created in our experiment. The ASW sample (c) crystallizes into stacking disordered ice when heated to a temperature of about 185 K with a 30 μs laser pulse (d), while hexagonal ice is mostly formed at about 235 K (e). When the sample is heated to about 281 K, it melts and vitrifies after the laser pulse to form HGW (f). The diffraction maxima are indicated with blue lines. Scale bars are 150 nm and 1 $Å^{-1}$.

studies that have shown that for aqueous solutions of cryoprotectants, the critical heating rate for outrunning crystallization is several orders of magnitude higher than the critical cooling rate.[26,27] However, these experiments were performed with high weight fractions of cryoprotectants to slow down crystallization, whereas no data are available for dilute solutions. Here, we characterize the melting process in amorphous ice samples of pure water with time-resolved electron diffraction.

Experiments are performed with a transmission electron microscope that we have modified for time-resolved experiments (supplementary material, Note 1).[28,29] As illustrated in Fig. 1(a), a 263 nm thick layer of amorphous solid water (ASW) is deposited *in situ* onto a sheet of few-layer graphene that is supported by a holey gold film (2 μm holes) on a 600 mesh gold grid held at 101 K. We then use a 30 μs laser pulse (532 nm) to melt the sample in the center of a grid square and probe its structural evolution by capturing a diffraction pattern with an intense, high-brightness electron pulse of 2 μs duration, containing about 10^5 electrons [Fig. 1(b)].

Figure 1(c) shows a micrograph of a typical ASW sample, with the corresponding diffraction pattern in the inset and the positions of the diffraction maxima indicated with blue lines (supplementary material, Note 12). When we heat the sample with a 30 μs laser pulse to about 185 K, it devitrifies and forms stacking disordered ice[30] [Fig. 1(d)], while at higher temperatures, the crystallization of hexagonal ice is favored[16,31] [Fig. 1(e), ~235 K, supplementary material, Note 11]. At even higher laser power, the sample melts and remains liquid for the duration of the laser pulse. Once the laser is switched off, the sample cools rapidly as the heat is efficiently dissipated to the surroundings, which have remained at cryogenic temperature.[3,11] With a cooling rate of over 10^7 K/s [see discussion in Fig. 2(a)], the sample vitrifies and forms HGW [Fig. 1(f)] after heating to 281 K. Note that the positions of the diffraction maxima of ASW in Fig. 1(c) are slightly shifted with respect to HGW. Such shifts are usually associated with the formation of microporous ASW, which is typically obtained at lower temperatures than in our experiment.[32,33] Contrast variations in the micrograph of Fig. 1(c) suggest that even

14 May 2024 05:17:49

© Author(s) 2024

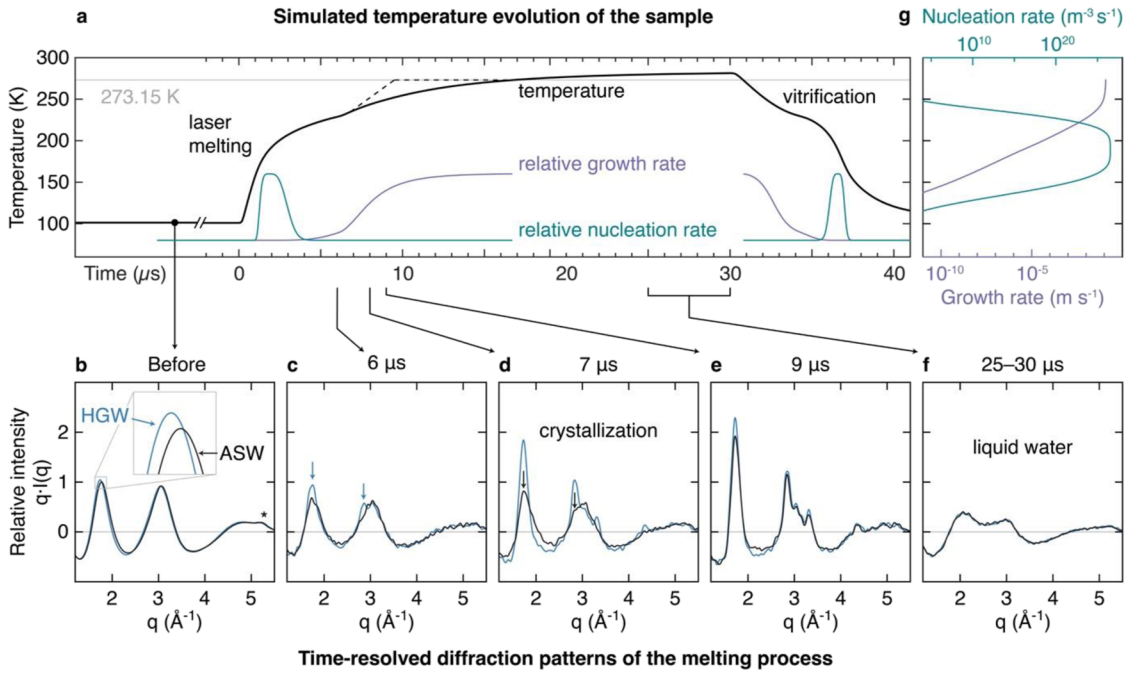

FIG. 2. Time-resolved diffraction patterns capture the structural evolution of the sample during the laser melting process. (a) Simulated temperature evolution of the sample (black). The dashed line schematically indicates the temperature evolution when the heat released by the partial crystallization of the sample is taken into account. The evolution of the relative nucleation and growth rates that the sample experiences during melting and vitrification are shown in green and purple, respectively (see also the discussion in the supplementary material, Note 9). (b)–(f) Time-resolved diffraction patterns (averages of at least 5 experiments) of the melting process for ASW (black) and HGW (blue). Arrows indicate the appearance of crystalline features. The asterisk in (b) marks a diffraction feature arising from the graphene support. (g) Absolute nucleation and growth rates (green and purple, respectively) as a function of temperature (supplementary material, Note 9).[1,39]

14 May 2024 05:17:49

under our deposition conditions, the samples exhibit a small amount of nanoscale porosity.

We characterize the structural evolution of the ASW sample during laser melting with time-resolved electron diffraction, with the diffraction pattern of the ASW sample before the laser pulse shown in Fig. 2(b) (black curve). For comparison, a simulation of the temperature evolution during this process is presented in Fig. 2(a) (black solid curve, supplementary material, Note 8). Under laser irradiation, the sample heats up rapidly, reaching a temperature of 229 K at 6 μs. The corresponding diffraction pattern reveals that the supercooled liquid has traversed most of no man's land without crystallization [Fig. 2(c)]. In contrast, additional diffraction features begin to appear at 7 μs (black arrows) that rapidly grow more intense [Fig. 2(e) and 9 μs], indicating the formation of stacking disordered ice and later, hexagonal ice (Fig. S7). Once the sample temperature reaches the melting point [16.8 μs in the simulation of Fig. 2(a)], the crystallites begin to melt, so that at long time delays, the diffraction pattern turns into that of stable water [Fig. 2(f), 25–30 μs]. We determine that at the end of the laser pulse, the sample reaches a temperature of 281 K (supplementary material, Note 7). Time-resolved diffraction patterns of the complete laser melting process are shown in Fig. S8. Note that, as discussed below, the simulation of the temperature evolution in Fig. 2(a) does not account for the heat released by the crystallization process during laser melting. This causes the sample to heat up more rapidly and approximately follow the temperature evolution indicated by the dashed line.

Our experiments reveal that crystallization occurs during melting but is avoided during vitrification, even though the respective heating and cooling rates are similar [Fig. 2(a)]. In fact, when crystallization sets in at about 6.8 μs (supplementary material, Note 6), the heating rate has not dropped below 5×10^6 K/s. This suggests that the critical heating rate of pure water is higher than the critical cooling rate, similar to solutions of cryoprotectants.[26,27] As has been previously discussed,[34] this can be qualitatively understood by considering how the nucleation and growth rates[1,39] [Fig. 2(g)] evolve during the melting and vitrification process [green and purple curves in Fig. 2(a); see also the discussion in the supplementary material, Note 9]. As the sample heats up, a large number of nuclei are formed in no man's land, where the nucleation rate goes through a maximum. At higher temperatures, nucleation slows significantly, but the growth rate picks up, causing the already existing nuclei to grow rapidly so that the sample crystallizes. In contrast, during the vitrification process, a large concentration of nuclei is only formed once the growth rate has already dropped. These nuclei will then grow only a little before the sample vitrifies and its structure is arrested.

Surprisingly, crystallization occurs significantly earlier when we repeat the experiment with the HGW sample that is obtained after the laser pulse [blue curves in Figs. 2(b)–2(f)]. Diffraction features indicating crystallization already appear at 6 μs [Fig. 2(c), blue

© Author(s) 2024

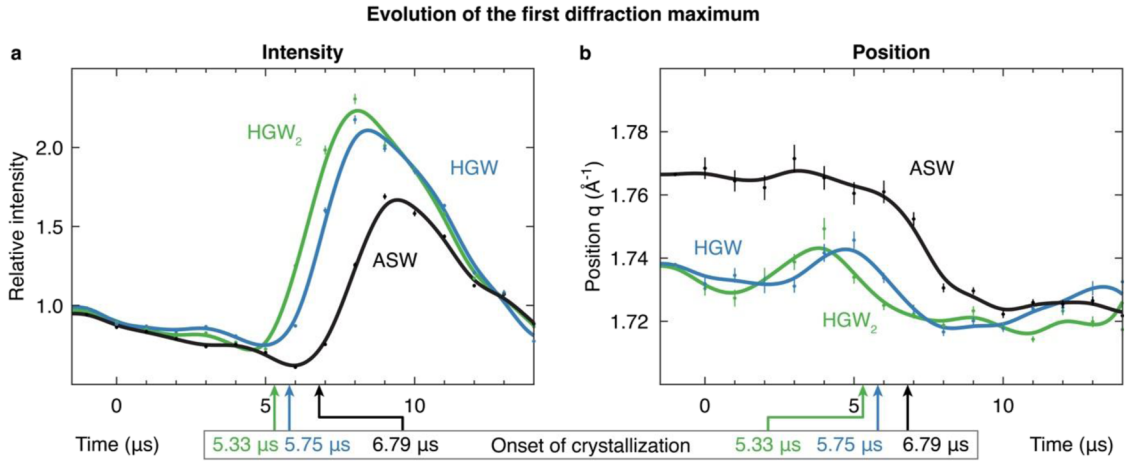

FIG. 3. Temporal evolution of the first diffraction maximum reveals the crystallization and structural relaxation dynamics of the sample. (a) Evolution of the diffraction intensity for ASW (black) and HGW (blue), as obtained after melting and vitrification of the ASW sample, as well as for HGW after melting and revitrifying a second time (HGW_2, green). (b) Evolution of the position of the diffraction maximum. The solid lines provide a guide to the eye and are derived from splines. Error bars indicate standard errors of the fit used to determine the intensities and positions.

arrows], after which they grow rapidly [Fig. 2(d)]. At the end of the laser pulse, the sample has fully melted, and its diffraction pattern is indistinguishable from that of the ASW sample [Fig. 2(f)]. The difference in crystallization kinetics is clearly evident in the evolution of the first diffraction maximum. Figure 3(a) shows that its intensity initially decreases as the sample heats up but rises sharply when crystallization sets in, which occurs at about 6.8 μs for ASW (black), but already at 5.8 μs for HGW (blue), 1 μs earlier (supplementary material, Note 6). This difference cannot be fully explained by the fact that the HGW sample is thinner due to evaporation during the first laser pulse and, therefore, heats up more rapidly. Simulations of the crystallization kinetics reveal that this effect can only account for a time delay of about 0.48 μs (supplementary material, Note 9). Indeed, when we laser melt the HGW sample a second time, it only crystallizes another 0.42 μs earlier [HGW_2, green data points in Fig. 3(a)]. The remaining time difference in the onset of crystallization between the ASW and HGW samples of over 0.5 μs must, therefore, result from a difference in the crystallization kinetics.

The intensity of the first diffraction peak goes through a maximum once the melting point is reached and crystal growth ceases, which occurs at ~8.0 μs for HGW_2, 8.5 μs for HGW, and 9.5 μs for ASW [Fig. 3(a)]. This is earlier than predicted by the simulation in Fig. 2(a) (solid line), which does not account for the heat released by the partial crystallization of the sample (16.8 μs). This heat release causes the sample to warm up more rapidly and follow a temperature evolution as sketched by the dashed line. From the time difference between the simulation and experiment for reaching the melting point, we can estimate that roughly a third of the sample crystallizes during laser melting (supplementary material, Note 10). Based on the relative diffraction intensities, we calculate that the maximum crystalline fraction of the HGW and HGW_2 samples is about 1.5 times as large as for ASW, a reflection of the faster crystallization kinetics of HGW.

The position of the first diffraction maximum provides insights into the structural evolution of the supercooled liquid before it crystallizes [Fig. 3(b)]. The first diffraction maximum of HGW (HGW_2) appears at 1.74 $Å^{-1}$, whereas that of ASW is shifted to 1.77 $Å^{-1}$ under our deposition conditions, as discussed above. During laser heating, the peak positions barely change until crystallization sets in, which is marked by a shift to lower momentum transfer, indicating the formation of stacking disordered ice, which features a strong reflection at 1.71 $Å^{-1}$ [Fig. 1(d)]. This suggests that the supercooled liquids obtained by laser heating ASW and HGW initially retain distinct structures. In particular, the ASW sample appears to partially preserve its nanoscale porosity. Nucleation, which predominantly takes place at lower temperatures [~140–230 K, Fig. 2(g)], must, therefore, occur in non-equilibrium configurations of supercooled water in our experiment. Evidently, the larger surface area of the ASW sample and the associated changes in local structure slow crystallization. This is in contrast to previous experiments on the crystallization of slowly heated amorphous ices, which found similar crystallization rates for ASW and HGW samples that were heated to 150 K.[35] Increasing the porosity of ASW was even shown to increase the crystallization rate in the temperature range of 130–141 K,[36] an observation that was ascribed to the associated larger surface area and the fact that surface nucleation dominates the crystallization process.[37,38] In our experiment, the nanoporous ASW sample instead crystallizes more slowly, which is likely a consequence of the flash heating process, which causes nucleation to predominantly occur at higher temperatures.

Based on simulations of the crystallization kinetics, we estimate an average nucleation rate of HGW in no man's land of 3.4×10^{26} m^{-3} s^{-1}, in rough agreement with previous measurements, while that of ASW is 6.6×10^{25} m^{-3} s^{-1}, about five times lower (supplementary material, Note 9). Note that our simulations can also reproduce the experimental observations if we instead assume a 1.7

14 May 2024 05:17:49

© Author(s) 2024

fold higher growth rate for HGW but an identical nucleation rate. We, therefore, cannot exclude that the observed difference in crystallization kinetics is in part due to the different growth rates of the two supercooled liquids. This is, however, unlikely to be the dominant contribution since the growth rate scales with diffusivity,[14,20,39] which intuitively should only weakly depend on changes in local structure.

In conclusion, our experiments reveal that during the rapid melting of ASW and HGW samples with microsecond laser pulses, about a third of the sample crystallizes, despite a heating rate of more than 5×10^6 K/s. In contrast, crystallization is avoided entirely under the same conditions during hyperquenching with a similar cooling rate of ~10^7 K/s. This can be understood by considering that as the sample heats up, it first undergoes fast nucleation before rapid growth sets in, whereas the opposite occurs during the vitrification process.[34] One can estimate an upper limit for the critical heating rate of 10^{10} K/s since crystallization can be outrun with 10 ns laser pulses.[19–21]

Our experiments open up the intriguing perspective of investigating how changes in local water structure affect the crystallization trajectory as well as the preference for the formation of different polymorphs.[40] For example, one would expect that preparing an amorphous ice precursor with an increased concentration of pentagonal rings would slow crystallization, which requires these rings to open and is, therefore, associated with a high energetic barrier.[41] Such experiments promise to help further elucidate the crystallization mechanism of water, which has remained an active area of research.[1,42,43]

We have previously shown that near-atomic resolution reconstructions can be obtained from revitrified cryo samples and that the structure of the proteins is not altered by the melting and revitrification processes.[25,44] The partial crystallization of the sample during the melting process, therefore, does not appear to negatively affect microsecond time-resolved cryo-EM experiments. If it did, it should always be possible to increase the heating rate and outrun crystallization by using a shaped laser pulse with an intense leading edge.[45] Transient crystallization during melting may, however, contribute to improving the sample quality by partially reshuffling the angular distribution of the particles[25] and, thus, help to overcome issues with preferred orientation that plague many cryo-EM projects.[46]

See the supplementary material for experimental methods, data analysis, and simulations, as well as time-resolved diffraction patterns of the complete flash melting process.

The authors would like to thank Dr. Pavel K. Olshin for his help with the heat transfer simulations as well as Dr. Jonathan M. Voss for his help with the preparation in Fig. 1.

This work was supported by the ERC Starting Grant No. 759145 as well as by the Swiss National Science Foundation Grant Nos. PP00P2,_163681, and 200020_207842.

AUTHOR DECLARATIONS

Conflict of Interest

The authors have no conflicts to disclose.

Author Contributions

N.J.M. C.R.K. G.B. These authors contributed equally.

Nathan J. Mowry: Data curation (equal); Formal analysis (equal); Investigation (equal); Methodology (equal); Writing – original draft (equal); Writing – review & editing (equal). **Constantin R. Krüger**: Data curation (equal); Formal analysis (equal); Investigation (equal); Methodology (equal); Writing – original draft (equal); Writing – review & editing (equal). **Gabriele Bongiovanni**: Data curation (equal); Formal analysis (equal); Investigation (equal); Methodology (equal); Writing – original draft (equal); Writing – review & editing (equal). **Marcel Drabbels**: Writing – review & editing (equal). **Ulrich J. Lorenz**: Conceptualization (lead); Supervision (lead); Writing – original draft (equal); Writing – review & editing (equal).

DATA AVAILABILITY

The data that support the findings of this study are openly available in Zenodo at https://doi.org/10.5281/zenodo.10624461.

REFERENCES

[1] P. Gallo *et al.*, "Water: A tale of two liquids," Chem. Rev. **116**, 7463–7500 (2016).
[2] P. H. Handle, T. Loerting, and F. Sciortino, "Supercooled and glassy water: Metastable liquid(s), amorphous solid(s), and a no-man's land," Proc. Natl. Acad. Sci. U. S. A. **114**, 13336–13344 (2017).
[3] C. R. Krüger, N. J. Mowry, G. Bongiovanni, M. Drabbels, and U. J. Lorenz, "Electron diffraction of deeply supercooled water in no man's land," Nat. Commun. **14**, 2812 (2023).
[4] M. Warkentin, J. P. Sethna, and R. E. Thorne, "Critical droplet theory explains the glass formability of aqueous solutions," Phys. Rev. Lett. **110**, 015703 (2013).
[5] I. Kohl, L. Bachmann, A. Hallbrucker, E. Mayer, and T. Loerting, "Liquid-like relaxation in hyperquenched water at ≤140 K," Phys. Chem. Chem. Phys. **7**, 3210 (2005).
[6] J. Dubochet, "Cryo-EM—the first thirty years," J. Microsc. **245**, 221–224 (2012).
[7] J. Dubochet and A. w. McDowall, "Vitrification of pure water for electron microscopy," J. Microsc. **124**, 3–4 (1981).
[8] P. Brüggeller and E. Mayer, "Complete vitrification in pure liquid water and dilute aqueous solutions," Nature **288**, 569–571 (1980).
[9] Y. Cheng, N. Grigorieff, P. A. Penczek, and T. Walz, "A primer to single-particle cryo-electron microscopy," Cell **161**, 438–449 (2015).
[10] E. Hand, "Cheap shots," Science **367**, 354–358 (2020).
[11] J. M. Voss, O. F. Harder, P. K. Olshin, M. Drabbels, and U. J. Lorenz, "Rapid melting and revitrification as an approach to microsecond time-resolved cryo-electron microscopy," Chem. Phys. Lett. **778**, 138812 (2021).
[12] J. M. Voss, O. F. Harder, P. K. Olshin, M. Drabbels, and U. J. Lorenz, "Microsecond melting and revitrification of cryo samples," Struct. Dyn. **8**, 054302 (2021).
[13] R. M. Glaeser, "Specimen behavior in the electron beam," Methods Enzymol. **579**, 19–50 (2016).
[14] G. A. Kimmel *et al.*, "Homogeneous ice nucleation rates and crystallization kinetics in transiently-heated, supercooled water films from 188 K to 230 K," J. Chem. Phys. **150**, 204509 (2019).
[15] L. Kringle, W. A. Thornley, B. D. Kay, and G. A. Kimmel, "Structural relaxation and crystallization in supercooled water from 170 to 260 K," Proc. Natl. Acad. Sci. U. S. A. **118**, e2022884118 (2021).
[16] M. Ladd-Parada *et al.*, "Following the crystallization of amorphous ice after ultrafast laser heating," J. Phys. Chem. B **126**, 2299–2307 (2022).

14 May 2024 05:17:49

© Author(s) 2024

[17]J. A. Sellberg *et al.*, "Ultrafast X-ray probing of water structure below the homogeneous ice nucleation temperature," Nature **510**, 381–384 (2014).
[18]H. Laksmono *et al.*, "Anomalous behavior of the homogeneous ice nucleation rate in 'no-man's land," J. Phys. Chem. Lett. **6**, 2826–2832 (2015).
[19]L. Kringle, W. A. Thornley, B. D. Kay, and G. A. Kimmel, "Reversible structural transformations in supercooled liquid water from 135 to 245 K," Science **369**, 1490–1492 (2020).
[20]Y. Xu, N. G. Petrik, R. S. Smith, B. D. Kay, and G. A. Kimmel, "Homogeneous nucleation of ice in transiently-heated, supercooled liquid water films," J. Phys. Chem. Lett. **8**, 5736–5743 (2017).
[21]Y. Xu *et al.*, "A nanosecond pulsed laser heating system for studying liquid and supercooled liquid films in ultrahigh vacuum," J. Chem. Phys. **144**, 164201 (2016).
[22]K. Amann-Winkel *et al.*, "Liquid-liquid phase separation in supercooled water from ultrafast heating of low-density amorphous ice," Nat. Commun. **14**, 442 (2023).
[23]K. H. Kim *et al.*, "Experimental observation of the liquid-liquid transition in bulk supercooled water under pressure," Science **370**, 978–982 (2020).
[24]O. F. Harder, S. V. Barrass, M. Drabbels, and U. J. Lorenz, "Fast viral dynamics revealed by microsecond time-resolved cryo-EM," Nat. Commun. **14**, 5649 (2023).
[25]G. Bongiovanni, O. F. Harder, J. M. Voss, M. Drabbels, and U. J. Lorenz, "Near-atomic resolution reconstructions from *in situ* revitrified cryo samples," Acta Crystallogr., Sect. D: Struct. Biol. **79**, 473–478 (2023).
[26]P. Boutron and P. Mehl, "Theoretical prediction of devitrification tendency: Determination of critical warming rates without using finite expansions," Cryobiology **27**, 359–377 (1990).
[27]Z. Han and J. C. Bischof, "Critical cooling and warming rates as a function of CPA concentration," CryoLetters **41**, 185–193 (2020).
[28]G. Bongiovanni, P. K. Olshin, M. Drabbels, and U. J. Lorenz, "Intense microsecond electron pulses from a Schottky emitter," Appl. Phys. Lett. **116**, 234103 (2020).
[29]P. K. Olshin, G. Bongiovanni, M. Drabbels, and U. J. Lorenz, "Atomic-resolution imaging of fast nanoscale dynamics with bright microsecond electron pulses," Nano Lett. **21**, 612–618 (2021).
[30]W. F. Kuhs, C. Sippel, A. Falenty, and T. C. Hansen, "Extent and relevance of stacking disorder in 'ice I_c," Proc. Natl. Acad. Sci. U. S. A. **109**, 21259–21264 (2012).
[31]K. Amann-Winkel *et al.*, "Water's second glass transition," Proc. Natl. Acad. Sci. U. S. A. **110**, 17720–17725 (2013).
[32]A. Hallbrucker, E. Mayer, and G. P. Johari, "Glass-liquid transition and the enthalpy of devitrification of annealed vapor-deposited amorphous solid water: A comparison with hyperquenched glassy water," J. Phys. Chem. **93**, 4986–4990 (1989).
[33]K. P. Stevenson, G. A. Kimmel, Z. Dohnálek, R. S. Smith, and B. D. Kay, "Controlling the morphology of amorphous solid water," Science **283**, 1505–1507 (1999).
[34]J. B. Hopkins, R. Badeau, M. Warkentin, and R. E. Thorne, "Effect of common cryoprotectants on critical warming rates and ice formation in aqueous solutions," Cryobiology **65**, 169–178 (2012).
[35]B. Maté, Y. Rodríguez-Lazcano, and V. J. Herrero, "Morphology and crystallization kinetics of compact (HGW) and porous (ASW) amorphous water ice," Phys. Chem. Chem. Phys. **14**, 10595 (2012).
[36]E. H. Mitchell, U. Raut, B. D. Teolis, and R. A. Baragiola, "Porosity effects on crystallization kinetics of amorphous solid water: Implications for cold icy objects in the outer solar system," Icarus **285**, 291–299 (2017).
[37]E. H. G. Backus, M. L. Grecea, A. W. Kleyn, and M. Bonn, "Surface crystallization of amorphous solid water," Phys. Rev. Lett. **92**, 236101 (2004).
[38]C. Yuan, R. S. Smith, and B. D. Kay, "Surface and bulk crystallization of amorphous solid water films: Confirmation of 'top-down' crystallization," Surf. Sci. **652**, 350–354 (2016).
[39]Y. Xu, N. G. Petrik, R. S. Smith, B. D. Kay, and G. A. Kimmel, "Growth rate of crystalline ice and the diffusivity of supercooled water from 126 to 262 K," Proc. Natl. Acad. Sci. U.S.A. **113**, 14921 (2016).
[40]M. Seidl, K. Amann-Winkel, P. H. Handle, G. Zifferer, and T. Loerting, "From parallel to single crystallization kinetics in high-density amorphous ice," Phys. Rev. B **88**, 174105 (2013).
[41]J. Russo and H. Tanaka, "Understanding water's anomalies with locally favoured structures," Nat. Commun. **5**, 3556 (2014).
[42]J. Russo, F. Romano, and H. Tanaka, "New metastable form of ice and its role in the homogeneous crystallization of water," Nat. Mater. **13**, 733–739 (2014).
[43]L. Lupi *et al.*, "Role of stacking disorder in ice nucleation," Nature **551**, 218–222 (2017).
[44]G. Bongiovanni, O. F. Harder, M. Drabbels, and U. J. Lorenz, "Microsecond melting and revitrification of cryo samples with a correlative light-electron microscopy approach," Front. Mol. Biosci. **9**, 1044509 (2022).
[45]C. R. Krüger, N. J. Mowry, M. Drabbels, and U. J. Lorenz, The Journal of Physical Chemistry Letters **15**(16), 4244–4248 (2024).
[46]R. M. Glaeser, "How good can cryo-EM become?," Nat. Methods **13**, 28–32 (2016).

14 May 2024 05:17:49

© Author(s) 2024